Self-energy of excited states in a strong Coulomb field

Peter J. Mohr and Yong-Ki Kim
National Institute of Standards and Technology, Gaithersburg, Maryland 20899
(Received 12 June 1991)

Results are given of a calculation of the self-energy radiative correction for electrons bound in a strong Coulomb field. The calculation has been done for the states with principal quantum number $n = 3$, 4, and 5, with angular momentum $j = \frac{1}{2}$ and $\frac{3}{2}$, and for nuclear charge Z in the range 10–110.

PACS number(s): 31.30.Jv, 12.20.Ds

I. INTRODUCTION

In many cases quantum electrodynamic (QED) corrections are an important component in the prediction of atomic energy levels. The dominant QED effects are the self-energy, corresponding to the virtual emission and reabsorption of photons by bound electrons, and the vacuum polarization, corresponding to interaction of virtual electron-positron pairs with the nucleus and bound electrons. This paper examines the one-photon self-energy, which is the largest radiative correction in most atoms.

The idealization that the electron is in the Coulomb field of a stationary point nucleus of charge Z is made in this work. This approximation provides the dominant effect for the theoretical predictions of hydrogenic energy levels [1, 2]. The Coulomb self-energy is also useful as a first approximation to radiative level shifts in highly ionized atoms and inner shells of heavy neutral atoms. In many cases the Coulomb-field result is the dominant contribution to the radiative level shift, and it is possible to estimate the effect of electron screening by perturbation theory [3].

Calculations of the self-energy in a strong Coulomb field for states with principal quantum number $n = 1$ and 2 with methods that form the basis for this work have been described previously [4–6]. Here, the calculations are extended to higher excited states with $n = 3$, 4, and 5, and with angular momentum $j = \frac{1}{2}$ and $\frac{3}{2}$, for nuclear charge Z in the range 10–110. Evaluation of the self-energy for higher-n states to high accuracy over this range of Z requires considerable improvement over the numerical methods employed for the $n = 1$ and 2 states, because the wave functions extend over a larger range in coordinate space and there is greater numerical cancellation in extracting the physical result from the formal expressions.

Preliminary results of the present work have been applied in a systematic study of regularities of resonance transitions along the lithium, sodium, and copper isoelectronic sequences with a phenomenological method of estimating the electron-screening effects on the self-energy [7].

Work has been done recently on the excited-state ($n \geq 3$) self-energy problem by Blundell and Snyderman [8] who employed a basis-set approach to calculate the Coulomb self-energy for a number of cases at high Z, including states with $n = 3$ and 4 at $Z = 80$. These results are compared to the present work in Sec. VI. Cheng, Johnson, and Sapirstein [9] have applied the method of Brown, Langer, and Schaefer [10] to calculate the self-energy in a local potential that approximates a Hartree-Fock potential for the $3s_{1/2}$ and $3p_{3/2}$ states at $Z = 78$ and the $4s_{1/2}$ and $4p_{3/2}$ states at $Z = 79$.

II. FORMULATION

The self-energy level shift $\Delta E_{\rm SE}$ can be written as the sum $\Delta E_{\rm SE} = \Delta E_L + \Delta E_H$ of a low-energy part ΔE_L and a high-energy part ΔE_H [4], where (in units in which $\hbar = c = m_e = 1$)

$$\Delta E_L = \frac{\alpha}{\pi} E_n - \frac{\alpha}{\pi} \mathrm{P} \int_0^{E_n} dz \int d\mathbf{x}_2 \int d\mathbf{x}_1 \phi_n^\dagger(\mathbf{x}_2) \alpha^j G(\mathbf{x}_2, \mathbf{x}_1, z) \alpha^l \phi_n(\mathbf{x}_1) (\delta_{jl} \boldsymbol{\nabla}_2 \cdot \boldsymbol{\nabla}_1 - \nabla_2^j \nabla_1^l) \frac{\sin[(E_n - z)x_{21}]}{(E_n - z)^2 x_{21}} \tag{2.1}$$

and

$$\Delta E_H = -\frac{i\alpha}{2\pi} \int_{C_H} dz \int d\mathbf{x}_2 \int d\mathbf{x}_1 \phi_n^\dagger(\mathbf{x}_2) \alpha_\mu G(\mathbf{x}_2, \mathbf{x}_1, z) \alpha^\mu \phi_n(\mathbf{x}_1) \frac{e^{-bx_{21}}}{x_{21}} - \delta m \int d\mathbf{x}\, \phi_n^\dagger(\mathbf{x}) \beta \phi_n(\mathbf{x}), \tag{2.2}$$

and where $b = -i\left[(E_n - z)^2 + i\delta\right]^{1/2}$, $\mathrm{Re}(b) > 0$, and $x_{21} = |\mathbf{x}_2 - \mathbf{x}_1|$. In these expressions, ϕ_n and E_n are the eigenfunction and eigenvalue of the Dirac equation for the bound state n with quantum numbers $\{n, \kappa_n, \mu_n\}$, and G is the Green's function for the Dirac equation corresponding to the operator $G = (H - z)^{-1}$, where H is the Dirac-Coulomb Hamiltonian. In (2.1) the P denotes principal value integration, and in (2.2) the contour C_H extends from $-i\infty$ to $0 - i\epsilon$ and from $0 + i\epsilon$ to $+i\infty$, with the appropriate branch of b chosen in each case. The explicit form of the coefficient δm in the mass-renormalization term in (2.2) depends on the regularization scheme that

is employed.

The division of the self-energy into (2.1) and (2.2) is done to facilitate the numerical evaluation. The low-energy part is amenable to high-precision evaluation with no subtraction terms, and the high-energy part is in the Feynman gauge in which subtractions done to isolate the infinite-mass renormalization have a simple form [4].

The self-energy level shift is roughly proportional to Z^4/n^3, so we express the results of the calculation in terms of a function $F(Z\alpha)$ defined by writing (in units of the electron rest energy $m_e c^2$)

$$\Delta E_{SE} = \frac{\alpha}{\pi}\frac{(Z\alpha)^4}{n^3}F(Z\alpha). \tag{2.3}$$

Because the low-energy and high-energy parts are separately of order lower than $(Z\alpha)^4$, it is useful to isolate the lower-order parts and define functions f_L and f_H that have the same scaling as F by writing [4, 6]

$$\Delta E_L = \frac{\alpha}{\pi}\left(\frac{3}{2}E_n + \frac{7}{6}V_n + \frac{(Z\alpha)^4}{n^3}f_L(Z\alpha)\right) \tag{2.4}$$

and

$$\Delta E_H = \frac{\alpha}{\pi}\left(-\frac{3}{2}E_n - \frac{7}{6}V_n + \frac{(Z\alpha)^4}{n^3}f_H(Z\alpha)\right), \tag{2.5}$$

where V_n is the expectation value of the Coulomb potential. In these expressions, the coefficients of E_n and V_n are obtained by evaluating the leading terms of (2.1) and (2.2) in powers of $Z\alpha$ analytically. The result for F is then simply

$$F(Z\alpha) = f_L(Z\alpha) + f_H(Z\alpha). \tag{2.6}$$

The value employed for the fine-structure constant in this work is $\alpha^{-1} = 137.036$.

III. LOW-ENERGY PART ΔE_L

Integration over the spherical angles of the vectors $\mathbf{x}_2$ and $\mathbf{x}_1$ in (2.1) yields [4]

$$\Delta E_L = \frac{\alpha}{\pi}E_n + \frac{\alpha}{\pi}\mathrm{P}\int_0^{E_n} dz\, u(z) \tag{3.1}$$

with

$$u(z) = -\int_0^\infty dx_2 x_2^2 \int_0^\infty dx_1 x_1^2 \sum_\kappa \sum_{i,j=1}^{2} f_{\bar{i}}(x_2) G_\kappa^{ij}(x_2, x_1, z) f_{\bar{j}}(x_1) A_\kappa^{ij}(x_2, x_1), \tag{3.2}$$

where the summation over κ runs over all nonzero integers, and where $\bar{i} = 3-i$ and $\bar{j} = 3-j$. Here ΔE_L is taken to be the real part of the corresponding symbol in Ref. [4]. In (3.2), the radial wave functions f_i (see Appendix A) and the radial Green's functions G_κ^{ij} are as defined in Ref. [4]. The functions A_κ^{ij} are given as an integral over the relative angle $\xi = \hat{\mathbf{x}}_2 \cdot \hat{\mathbf{x}}_1$ in Ref. [4] for any state, and the result of the integration is given for $S_{1/2}$ states in Ref. [4], for $P_{1/2}$ and $P_{3/2}$ states in Ref. [6], and for $D_{3/2}$ states in Appendix B of this paper. The function $u(z)$ in (3.2) is evaluated numerically with methods similar to those described in Refs. [5] and [6]. In this calculation, minor modifications in the algorithms for evaluating the radial Green's functions have been made in order to extend the range to the higher values of z needed here. In most cases, the integration over radial coordinates is carried out by a method described earlier, except that here higher-order Gaussian integration formulas are employed. In some cases, to obtain convergence, an alternative integration scheme was employed. The modification is that the ranges (0,1), (1,5), and (5,∞) corresponding to the three terms in Eq. (2.20) of Ref. [5] are replaced by (0,n), (n,5n), and (5n,∞), where n is the principal quantum number of the state, with a nominal number of integration points given by 34, 18, and 6, respectively.

In evaluating the integral over $u(z)$, it is necessary to take into account the fact that the integrand $u(z)$ in (3.2) contains as many as 11 bound-state poles within the range of integration for the states considered here. We subtract the pole terms from the integrand when integrating over z, and add the result of analytically integrating these terms to restore the correct value for the integral. Locations and residues of the poles of $u(z)$ are readily identified with the aid of the spectral resolution of the radial Green's function

$$G_\kappa^{ij}(x_2, x_1, z) = \sum_m \frac{f_i(x_2) f_j(x_1)}{E_m - z}. \tag{3.3}$$

In (3.3), the summation over m denotes summation over principal quantum numbers m of all bound states and integration over the continuous-energy spectrum for a fixed spin-orbital quantum number κ. To be explicit, both the bound-state energy eigenvalues and radial wave functions depend on m and κ as well as the displayed variables, i.e., $f_i(x) = f_{m,\kappa,i}(x)$ and $E_m = E_{m,\kappa}$. Pole terms are isolated by writing

$$u(z) = \sum_{\substack{m,\kappa \\ E_{m,\kappa} < E_{n,\kappa_n}}} \frac{R_{m,\kappa}}{z - E_{m,\kappa}} + v(z), \tag{3.4}$$

where $v(z)$ is analytic on the interval $(0, E_n)$ and

$$R_{m,\kappa} = \int_0^\infty dx_2 x_2^2 \int_0^\infty dx_1 x_1^2 \sum_{i,j=1}^{2} f_{n,\kappa_n,\bar{i}}(x_2) f_{m,\kappa,i}(x_2) f_{m,\kappa,j}(x_1) f_{n,\kappa_n,\bar{j}}(x_1) \left[A_\kappa^{ij}(x_2, x_1)\right]_{z=E_{m,\kappa}}. \tag{3.5}$$

To numerically evaluate the principal-value integration over z, we calculate the residues $R_{m,\kappa}$ by numerically evaluating (3.5), and integrate the modified integrand $\bar{u}(z)$ defined by

$$\bar{u}(z) = u(z) + \sum_{\substack{m,\kappa \\ E_{m,\kappa} < E_{n,\kappa_n}}} R_{m,\kappa} \left[\frac{1}{E_{n,\kappa_n}} \ln \left(\frac{E_{n,\kappa_n} - E_{m,\kappa}}{E_{m,\kappa}} \right) - \frac{1}{z - E_{m,\kappa}} \right] \tag{3.6}$$

by standard Gaussian quadrature, i.e.,

$$\mathrm{P} \int_0^{E_n} dz\, u(z) = \int_0^{E_n} dz\, \bar{u}(z). \tag{3.7}$$

Each radial integral in (3.5) is evaluated by Gaussian quadrature. The method consists of dividing the range of integration into two parts and making changes of variables defined by

$$\int_0^\infty dx\, g(x) = \int_0^1 dx\, \frac{18x^2}{a}\, g\left(\frac{6x^3}{a}\right) + \int_0^\infty dx\, \frac{1}{a}\, g\left(\frac{x+6}{a}\right), \tag{3.8}$$

where $a = (1 - E_{n,\kappa_n}^2)^{1/2} + (1 - E_{m,\kappa}^2)^{1/2}$, with the first integral on the right-hand side evaluated with 22-point Gauss-Legendre quadrature, and the second integral on the right-hand side evaluated with 12-point Gauss-Laguerre quadrature. The parameter a is defined so that the integrand of the second integral falls off as $x^q e^{-x}$, for large x. The division and changes of variables in (3.8) are the result of a trial and error effort to obtain high precision in the numerical integration with a minimum number of integration points. Error introduced into the final result from error in the residue calculation was checked by increasing the number of integration points by 10 in each integral in the residue calculation for representative values of n and Z. The change in the result, $f_L(Z\alpha)$, was less than 3×10^{-8} in all cases.

For $|\kappa_n| = 1$, the integral on the right-hand side of (3.7) is evaluated by Gauss-Legendre quadrature with respect to a new variable t defined by

$$\int_0^{E_n} dz\, \bar{u}(z) = \int_0^1 dt\, 5E_n t^4\, \bar{u}(E_n(1 - t^5)) \tag{3.9}$$

with the nominal number of integration points given by 18. In the cases where $|\kappa_n| = 2$, we divide the integral over z into two regions with the division point given by

$$z_0 = 2E_{n,1} - E_{n,2}, \tag{3.10}$$

where $E_{n,1}$ is the nearby eigenvalue with $|\kappa| = 1$. With this point of division, the upper interval is symmetric about the pole at $z = E_{n,1}$, and the convergence of the integral over z as the number of integration points is increased is better than if no division were made. In fact, in most of the evaluations, this nearest pole was not subtracted. By the choice of integration intervals, the principal-value integral is evaluated correctly with or without the subtraction, as discussed in Ref. [6]. The method of integration is given by

$$\int_0^{E_n} dz \bar{u}(z) = \int_0^1 dt\, 5z_0 t^4\, \bar{u}(z_0(1 - t^5)) + \int_0^1 dt\, (E_n - z_0)\bar{u}(E_n - (E_n - z_0)t), \tag{3.11}$$

where the integrals over t are evaluated by Gaussian quadrature with a nominal number of points given by 18 and 4, respectively, for the two intervals.

Results of this evaluation for the function $f_L(Z\alpha)$ are shown in Tables I–III. The stability of the results as the number of integration points in all dimensions is varied is taken as an indication of the precision in the values, and the uncertainty in the last figure is shown in parentheses in the cases where it is not negligible. The quoted results are based on a number of integration points in the range 4 to 10 greater than the nominal number for each integral.

IV. HIGH-ENERGY ANALYTIC PART

The high-energy part ΔE_H is divided into two parts so that

$$f_H(Z\alpha) = f_{HA}(Z\alpha) + f_{HB}(Z\alpha). \tag{4.1}$$

In Ref. [6], the analytic part $f_{HA}(Z\alpha)$ is defined for any state in terms of expectation values in momentum

TABLE I. The function $f_L(Z\alpha)$ for $n = 3$.

Z	$3S_{1/2}$	$3P_{1/2}$	$3P_{3/2}$	$3D_{3/2}$
10	6.364420	1.014106	0.753842	0.489050
20	4.906471	1.055303	0.770811	0.491722
30	4.180915	1.113925	0.792782	0.496067
40	3.750657	1.189990	0.818598	0.502184
50	3.484073	1.285831	0.847813	0.510245
60	3.327107	1.406028	0.880348	0.520484
70	3.256334	1.558249	0.916373	0.533206
80	3.265610	1.755248	0.956255	0.548806
90	3.364248	2.019312	1.000532	0.567792
100	3.584845	2.393137	1.049879	0.590822
110	4.013497	2.971636	1.105008	0.618746

TABLE II. The function $f_L(Z\alpha)$ for $n = 4$.

Z	$4S_{1/2}$	$4P_{1/2}$	$4P_{3/2}$	$4D_{3/2}$
10	6.40884(1)	1.04173(1)	0.781412(3)	0.513346(3)
20	4.947659	1.083388	0.799114	0.516252
30	4.217650	1.142055	0.822071	0.520971
40	3.781679	1.217436	0.849134	0.527658
50	3.507808	1.311451	0.879887	0.536537
60	3.341405	1.428082	0.914309	0.547910
70	3.258091	1.574052	0.952652	0.562172
80	3.250127	1.760529	0.995399	0.579837
90	3.323999	2.006924	1.043231	0.601571
100	3.506800	2.350188	1.096993	0.628249
110	3.872100	2.871950	1.157550	0.661005

TABLE III. The function $f_L(Z\alpha)$ for $n = 5$.

Z	$5S_{1/2}$	$5P_{1/2}$	$5P_{3/2}$	$5D_{3/2}$
10	6.4328(1)	1.05789(5)	0.79761(2)	0.52780(2)
20	4.968871	1.099472	0.815590	0.530791(1)
30	4.235040	1.157583	0.838843	0.535587
40	3.794169	1.231728	0.866243	0.542399
50	3.514102	1.323523	0.897378	0.551473
60	3.339795	1.436505	0.932239	0.563139
70	3.246190	1.576704	0.971102	0.577828
80	3.224427	1.754146	1.014480	0.596102
90	3.279036	1.986220	1.063097	0.618692
100	3.433348	2.305937	1.117841	0.646561
110	3.752487	2.786047	1.179589	0.680957

space. Momentum-space functions that are required for this calculation are given in Appendix A. Reference [6] describes the method of evaluation. Results for the function $f_{HA}(Z\alpha)$ are listed in Tables IV–VI. None of the figures in those tables is affected by numerical uncertainty.

V. HIGH-ENERGY REMAINDER

The high-energy remainder function $f_{HB}(Z\alpha)$ is

$$f_{HB}(\gamma) = \int_0^1 dt \int_0^\infty dy \int_0^1 dr\, S(r,y,t,\gamma), \tag{5.1}$$

where

$$S(r,y,t,\gamma) = \sum_{\kappa=1}^{\infty} T_\kappa(r,y,t,\gamma). \tag{5.2}$$

The terms $T_\kappa(r,y,t,\gamma)$ are defined in Ref. [6]. In this calculation, the summation in (5.2) is done by directly evaluating the sum for $\kappa \le N$ and adding an asymptotic estimate for the remainder. In particular, the evaluation procedure is based on the expression

$$S(r,y,t,\gamma) = S_N + R_N + E_N, \tag{5.3}$$

where S_N is the partial sum

$$S_N = \sum_{\kappa=1}^{N} T_\kappa(r,y,t,\gamma), \tag{5.4}$$

TABLE IV. The function $f_{HA}(Z\alpha)$ for $n = 3$.

Z	$3S_{1/2}$	$3P_{1/2}$	$3P_{3/2}$	$3D_{3/2}$
10	−1.474363	−1.155076	−0.593190	−0.524572
20	−1.478201	−1.173638	−0.596242	−0.526929
30	−1.499892	−1.205890	−0.601288	−0.530902
40	−1.539393	−1.254001	−0.608338	−0.536561
50	−1.598280	−1.321461	−0.617427	−0.544002
60	−1.679913	−1.413709	−0.628625	−0.553361
70	−1.790203	−1.539318	−0.642027	−0.564808
80	−1.939349	−1.712301	−0.657762	−0.578562
90	−2.145774	−1.957012	−0.675993	−0.594893
100	−2.445939	−2.319978	−0.696926	−0.614143
110	−2.923713	−2.904165	−0.720816	−0.636731

TABLE V. The function $f_{HA}(Z\alpha)$ for $n = 4$.

Z	$4S_{1/2}$	$4P_{1/2}$	$4P_{3/2}$	$4D_{3/2}$
10	−1.507887	−1.188710	−0.627128	−0.558512
20	−1.510582	−1.206432	−0.630281	−0.560976
30	−1.530295	−1.237178	−0.635495	−0.565132
40	−1.566819	−1.282939	−0.642780	−0.571049
50	−1.621450	−1.346895	−0.652176	−0.578832
60	−1.697093	−1.433976	−0.663758	−0.588620
70	−1.798916	−1.551886	−0.677630	−0.600593
80	−1.935872	−1.713108	−0.693929	−0.614978
90	−2.124120	−1.939137	−0.712832	−0.632056
100	−2.395577	−2.270624	−0.734561	−0.652179
110	−2.823389	−2.796620	−0.759391	−0.675781

R_N is the remainder estimate, and E_N is the error. For large κ, the asymptotic form of the terms is

$$T_\kappa(r,y,t,\gamma) = \frac{r^{2\kappa}}{\kappa} P_\kappa(r,y,t,\gamma), \tag{5.5}$$

where

$$P_\kappa(r,y,t,\gamma) = A(r,y,t,\gamma) + B(r,y,t,\gamma)\frac{1}{(\kappa+1)} + O\left(\frac{1}{\kappa^2}\right). \tag{5.6}$$

To construct the remainder estimate R_N, we calculate the term $A(r,y,t,\gamma)$ analytically with the aid of the asymptotic expression for the radial Green's function in Ref. [5], and approximate $B(r,y,t,\gamma)$ by

$$\bar{B}_N(r,y,t,\gamma) = (N+1)\,[P_N(r,y,t,\gamma) - A(r,y,t,\gamma)], \tag{5.7}$$

so that

$$\bar{B}_N(r,y,t,\gamma) = B(r,y,t,\gamma) + O\left(\frac{1}{N}\right). \tag{5.8}$$

The remainder estimate is defined to be

$$R_N = A_N + B_N, \tag{5.9}$$

where

$$A_N = A(r,y,t,\gamma) \sum_{\kappa=N+1}^{\infty} \frac{r^{2\kappa}}{\kappa} \tag{5.10}$$

TABLE VI. The function $f_{HA}(Z\alpha)$ for $n = 5$.

Z	$5S_{1/2}$	$5P_{1/2}$	$5P_{3/2}$	$5D_{3/2}$
10	−1.527916	−1.208819	−0.647463	−0.578850
20	−1.529664	−1.225817	−0.650590	−0.581301
30	−1.547741	−1.255278	−0.655758	−0.585433
40	−1.581815	−1.299059	−0.662973	−0.591316
50	−1.632969	−1.360113	−0.672274	−0.599052
60	−1.703768	−1.442998	−0.683730	−0.608775
70	−1.798842	−1.554800	−0.697438	−0.620661
80	−1.926236	−1.706935	−0.713530	−0.634931
90	−2.100502	−1.918933	−0.732174	−0.651856
100	−2.350376	−2.227500	−0.753579	−0.671776
110	−2.741625	−2.712543	−0.778007	−0.695108

and

$$B_N = \bar{B}_N(r,y,t,\gamma) \sum_{\kappa=N+1}^{\infty} \frac{r^{2\kappa}}{\kappa(\kappa+1)}. \tag{5.11}$$

The sums in (5.10) and (5.11) are evaluated numerically with the aid of the identities

$$\sum_{\kappa=N+1}^{\infty} \frac{r^{2\kappa}}{\kappa} = \ln\left(\frac{1}{1-r^2}\right) - \sum_{\kappa=1}^{N} \frac{r^{2\kappa}}{\kappa} \tag{5.12}$$

and

$$\sum_{\kappa=N+1}^{\infty} \frac{r^{2\kappa}}{\kappa(\kappa+1)} = 1 - \frac{1-r^2}{r^2} \ln\left(\frac{1}{1-r^2}\right) - \sum_{\kappa=1}^{N} \frac{r^{2\kappa}}{\kappa(\kappa+1)}. \tag{5.13}$$

The error is expected to have a smaller magnitude than the second remainder term

$$|E_N| < |B_N|, \tag{5.14}$$

which was determined empirically to be a reliable estimate. In fact, this estimate is found to be conservative, as would be expected from the fact that the second remainder term B_N is included in the calculated value for the sum. The cutoff N is fixed by summing the series in (5.2) until all of the conditions

$$|B_{N-2}| < \epsilon, \quad |B_{N-1}| < \epsilon, \quad |B_N| < \epsilon \tag{5.15}$$

are satisfied. The error bound ϵ is taken to be

$$\epsilon = \begin{cases} 10^{-4} & \text{for } \kappa > \kappa_a \\ 10^{-5} & \text{otherwise,} \end{cases} \tag{5.16}$$

where

$$\kappa_a = \max(5, 1.5w, 1.5(1-r)w^2) - 1 \tag{5.17}$$

and

$$w = \frac{(1+t^2)y}{4t(1-E_n^2)^{1/2}}. \tag{5.18}$$

The limit κ_a is roughly the minimum value of κ for which the asymptotic forms employed in the remainder and error estimate are valid. The second line in (5.16) corresponds to termination of the sum before κ reaches the asymptotic region. In this case, the falloff of the terms is generally dominated by the factor $r^{2\kappa}$ rather than inverse powers of κ. The number of terms required to meet the cutoff condition ranged to a maximum of about 50 000.

The validity of this evaluation procedure was checked by comparing the calculated result $f_{HB}(Z\alpha)$, in a representative sample of evaluations, to the more precise result obtained either by reducing the error bound ϵ by one or two orders of magnitude or by extending the summation and remainder calculation ten terms beyond the value of N determined by (5.15). In each case, the modified result differed from the unmodified result by less than 10^{-4}, and in most comparisons the difference was in the range 10^{-5} to 10^{-6}.

The multiple integral shown in (5.1) is evaluated as follows. In the y integration, the variable is changed to $w = py$, where

$$p = 1 + \frac{1-r}{2}\left(\frac{1}{t(1-E_n^2)^{1/2}} - 1\right), \tag{5.19}$$

so that the integrand S falls off exponentially as e^{-w} for large w. The range of integration is then divided into two parts with the division point w_0, given by

$$w_0 = 2n, \tag{5.20}$$

where n is the principal quantum number of the state. The variable in the region $w < w_0$ is scaled to the range (0,1), and the variable in the region $w > w_0$ is translated to the range (0,∞). Finally, the variable in the range (0,1) is defined to be the third power of a new variable. The changes are summarized by writing

$$\begin{aligned} S_1(r,t,\gamma) &= \int_0^{\infty} dy\, S(r,y,t,\gamma) \\ &= \frac{3w_0}{p}\int_0^1 dx\, x^2 S\left(r, \frac{w_0 x^3}{p}, t, \gamma\right) \\ &\quad + \frac{1}{p}\int_0^{\infty} dx\, S\left(r, \frac{w_0+x}{p}, t, \gamma\right). \end{aligned} \tag{5.21}$$

Integration over (0,1) is evaluated by Gauss-Legendre quadrature initially with N_1 integration points, and the integration over (0,∞) is evaluated by Gauss-Laguerre quadrature, initially with N_2 integration points. The values of N_1 and N_2 depend on n, Z, r, and t, and are shown in Table VII. Final results are obtained by increasing the number of points in the quadrature formulas in all dimensions until satisfactory convergence is obtained.

The integrals over r and t are evaluated by Gauss-Legendre quadrature with various variable changes and initial numbers of points. For $Z > 60$, the integral over r

$$S_2(t,\gamma) = \int_0^1 dr\, S_1(r,t,\gamma) \tag{5.22}$$

is evaluated directly with ten integration points, and the integral over t is evaluated with a new variable x

$$S_3(\gamma) = 2\int_0^1 dx\, x\, S_2(x^2,\gamma) \tag{5.23}$$

with ten integration points. When $Z \leq 60$, the integral over r is divided into three intervals (0,0.9), (0.9,0.99), and (0.99,1), and the method of integration over t depends on the interval. The quadrature formulas are applied to the expression

TABLE VII. Values for the numbers N_1 and N_2. $[x]$ denotes the largest integer less than or equal to x.

Z	r	N_1	N_2
≤ 60	(0, 0.9)	$5+2n$	3
≤ 60	(0.9, 0.99)	$6+[12t]$	$3+[80(r-0.9)t]$
≤ 60	(0.99, 1)	$12+[6t]$	$3+[4t]$
> 60	(0, 1)	$5+2n$	3

TABLE VIII. The function $f_{HB}(Z\alpha)$ for $n = 3$.

Z	$3S_{1/2}$	$3P_{1/2}$	$3P_{3/2}$	$3D_{3/2}$
10	0.0624(2)	0.0389(2)	−0.0186(2)	−0.0072(2)
20	0.1350(1)	0.0423(1)	−0.0174(1)	−0.0068(1)
30	0.2129(1)	0.0489(1)	−0.0154(1)	−0.0062(1)
40	0.2970(1)	0.0599(1)	−0.0125(1)	−0.0052(1)
50	0.3899(1)	0.0770(1)	−0.0089(1)	−0.0040(1)
60	0.4959(1)	0.1033(1)	−0.0047(1)	−0.0025(1)
70	0.6212(1)	0.1434(1)	0.0001(1)	−0.0005(1)
80	0.7755(1)	0.2054(1)	0.0053(1)	0.0018(1)
90	0.9751(1)	0.3037(1)	0.0104(1)	0.0046(1)
100	1.2508(1)	0.4676(1)	0.0150(1)	0.0079(1)
110	1.6711(1)	0.7647(1)	0.0178(1)	0.0118(1)

TABLE X. The function $f_{HB}(Z\alpha)$ for $n = 5$.

Z	$5S_{1/2}$	$5P_{1/2}$	$5P_{3/2}$	$5D_{3/2}$
10	0.0809(6)	0.0576(6)	0.0001(6)	0.0115(6)
20	0.1531(2)	0.0611(4)	0.0012(1)	0.0119(1)
30	0.2300(1)	0.0678(1)	0.0031(1)	0.0124(1)
40	0.3122(1)	0.0789(1)	0.0057(1)	0.0133(1)
50	0.4022(1)	0.0963(1)	0.0090(1)	0.0144(1)
60	0.5035(1)	0.1226(1)	0.0129(1)	0.0159(1)
70	0.6213(1)	0.1624(1)	0.0173(1)	0.0177(1)
80	0.7637(1)	0.2231(1)	0.0220(1)	0.0198(1)
90	0.9439(1)	0.3176(1)	0.0265(1)	0.0224(1)
100	1.1867(1)	0.4713(1)	0.0303(1)	0.0253(1)
110	1.5458(1)	0.7415(1)	0.0322(1)	0.0286(1)

$$S_3(\gamma) = 1.8 \int_0^1 du\, u \int_0^1 dx\, S_1(0.9x, u^2, \gamma) + 0.09 \int_0^1 dt \int_0^1 dx\, S_1(0.9 + 0.09x, t, \gamma) + 0.01 \int_0^1 dt \int_0^1 dx\, S_1(0.99 + 0.01x, t, \gamma), \tag{5.24}$$

with 10 × 10, 6 × 8, and 4 × 4 integration points, respectively. Results of the calculation for $f_{HB}(Z\alpha)$ appear in Tables VIII–X. The quoted numbers are the result of evaluating the integrals as described above with the number of additional integration points in each dimension ranging from 4 to 8. In the tables, the numbers in parentheses are estimated uncertainties in the last figure shown based on the apparent convergence of the numerical integration. The estimated uncertainty is expected to be larger than the actual error in the number in most cases.

VI. CONCLUSION

Results of this calculation are summarized as values of the function $F(Z\alpha)$ shown in Tables XI–XIII. The level shift follows from this function as shown in (2.3).

Results of this calculation are compared to the work of Blundell and Snyderman [8] in terms of the function $F(Z\alpha)$ in Table XIV. There is agreement between the two calculations.

The excited-state self-energy for a given angular momentum is shown in the graphs for $S_{1/2}$ states in Fig. 1, for $P_{1/2}$ states in Fig. 2, for $P_{3/2}$ states in Fig. 3, and for $D_{3/2}$ states in Fig. 4. Curves for a given κ and different n exhibit a remarkable degree of similarity as functions of Z, apparently approaching an asymptotic limit as n increases. This corresponds to an asymptotic n^{-3} behavior of the level shifts for any Z. Another trend in the results is that both the magnitude and relative Z dependence of the functions $F(Z\alpha)$ decrease as j and l increase. These properties are associated with the fact that the self-energy correction is sensitive to the electron wave function within a distance of the order of the Compton wavelength of the electron from the nucleus.

APPENDIX A

For completeness, the known expressions for the coordinate-space and momentum-space Dirac-Coulomb wave functions are reproduced here in the general form employed in this calculation. The coordinate-space radial wave functions $f_1(x)$ and $f_2(x)$ are defined by [11]

TABLE IX. The function $f_{HB}(Z\alpha)$ for $n = 4$.

Z	$4S_{1/2}$	$4P_{1/2}$	$4P_{3/2}$	$4D_{3/2}$
10	0.0740(4)	0.0507(4)	−0.0065(4)	0.0049(4)
20	0.1463(1)	0.0541(2)	−0.0058(1)	0.0048(1)
30	0.2236(1)	0.0608(1)	−0.0039(1)	0.0054(1)
40	0.3066(1)	0.0719(1)	−0.0012(1)	0.0063(1)
50	0.3979(1)	0.0892(1)	0.0022(1)	0.0075(1)
60	0.5012(1)	0.1157(1)	0.0062(1)	0.0090(1)
70	0.6222(1)	0.1559(1)	0.0108(1)	0.0108(1)
80	0.7698(1)	0.2174(1)	0.0156(1)	0.0130(1)
90	0.9583(1)	0.3141(1)	0.0203(1)	0.0156(1)
100	1.2150(1)	0.4730(1)	0.0243(1)	0.0187(1)
110	1.5997(1)	0.7557(1)	0.0265(1)	0.0221(1)

TABLE XI. The function $F(Z\alpha)$ for $n = 3$.

Z	$3S_{1/2}$	$3P_{1/2}$	$3P_{3/2}$	$3D_{3/2}$
10	4.9524(2)	−0.1021(2)	0.1421(2)	−0.0428(2)
20	3.5633(1)	−0.0760(1)	0.1572(1)	−0.0420(1)
30	2.8940(1)	−0.0430(1)	0.1761(1)	−0.0410(1)
40	2.5083(1)	−0.0041(1)	0.1977(1)	−0.0396(1)
50	2.2757(1)	0.0414(1)	0.2214(1)	−0.0378(1)
60	2.1431(1)	0.0956(1)	0.2470(1)	−0.0353(1)
70	2.0874(1)	0.1623(1)	0.2745(1)	−0.0321(1)
80	2.1018(1)	0.2483(1)	0.3038(1)	−0.0279(1)
90	2.1935(1)	0.3660(1)	0.3350(1)	−0.0225(1)
100	2.3897(1)	0.5408(1)	0.3679(1)	−0.0154(1)
110	2.7609(1)	0.8322(1)	0.4020(1)	−0.0062(1)

TABLE XII. The function $F(Z\alpha)$ for $n = 4$.

Z	$4S_{1/2}$	$4P_{1/2}$	$4P_{3/2}$	$4D_{3/2}$
10	4.9749(4)	−0.0963(4)	0.1477(4)	−0.0403(4)
20	3.5834(1)	−0.0690(2)	0.1630(1)	−0.0399(1)
30	2.9110(1)	−0.0344(1)	0.1827(1)	−0.0387(1)
40	2.5215(1)	0.0064(1)	0.2052(1)	−0.0371(1)
50	2.2842(1)	0.0538(1)	0.2299(1)	−0.0348(1)
60	2.1455(1)	0.1098(1)	0.2568(1)	−0.0317(1)
70	2.0814(1)	0.1780(1)	0.2858(1)	−0.0276(1)
80	2.0840(1)	0.2649(1)	0.3170(1)	−0.0222(1)
90	2.1582(1)	0.3819(1)	0.3507(1)	−0.0149(1)
100	2.3262(1)	0.5525(1)	0.3868(1)	−0.0053(1)
110	2.6484(1)	0.8311(1)	0.4247(1)	0.0074(1)

$$\phi(\mathbf{x}) = \begin{pmatrix} f_1(x)\chi_\kappa^\mu(\hat{\mathbf{x}}) \\ i f_2(x)\chi_{-\kappa}^\mu(\hat{\mathbf{x}}) \end{pmatrix}. \tag{A1}$$

We employ the notation

$$\gamma = Z\alpha, \quad \lambda = (\kappa^2 - \gamma^2)^{1/2},$$
$$n_r = n - |\kappa|, \quad a = \frac{\gamma}{[(n_r + \lambda)^2 + \gamma^2]^{1/2}}, \tag{A2}$$

with the bound-state energy given by $E = (1 - a^2)^{1/2}$. The normalization factor is

$$N = \frac{2a^5}{\gamma(\gamma - \kappa a)} \frac{\Gamma(2\lambda + 1 + n_r)}{\Gamma(2\lambda + 1)^2 \Gamma(n_r + 1)}, \tag{A3}$$

and a set of coefficients is defined recursively by

$$C_1^{(m+1)} = \frac{m + 1 - n_r}{(m + 2\lambda + 1)(m + 1)} C_1^{(m)} \tag{A4}$$

and

$$C_2^{(m+1)} = \frac{m - n_r}{(m + 2\lambda + 1)(m + 1)} C_2^{(m)}, \tag{A5}$$

with initial values

$$C_1^{(0)} = -n_r, \qquad C_2^{(0)} = \frac{\gamma}{a} - \kappa. \tag{A6}$$

In terms of these coefficients, the radial wave functions are

TABLE XIII. The function $F(Z\alpha)$ for $n = 5$.

Z	$5S_{1/2}$	$5P_{1/2}$	$5P_{3/2}$	$5D_{3/2}$
10	4.9858(6)	−0.0933(6)	0.1502(6)	−0.0396(6)
20	3.5923(2)	−0.0652(4)	0.1662(1)	−0.0387(1)
30	2.9173(1)	−0.0299(1)	0.1861(1)	−0.0374(1)
40	2.5246(1)	0.0116(1)	0.2089(1)	−0.0356(1)
50	2.2833(1)	0.0597(1)	0.2341(1)	−0.0331(1)
60	2.1395(1)	0.1161(1)	0.2614(1)	−0.0297(1)
70	2.0686(1)	0.1843(1)	0.2910(1)	−0.0252(1)
80	2.0619(1)	0.2703(1)	0.3229(1)	−0.0190(1)
90	2.1225(1)	0.3848(1)	0.3574(1)	−0.0108(1)
100	2.2696(1)	0.5497(1)	0.3946(1)	0.0001(1)
110	2.5566(1)	0.8150(1)	0.4338(1)	0.0145(1)

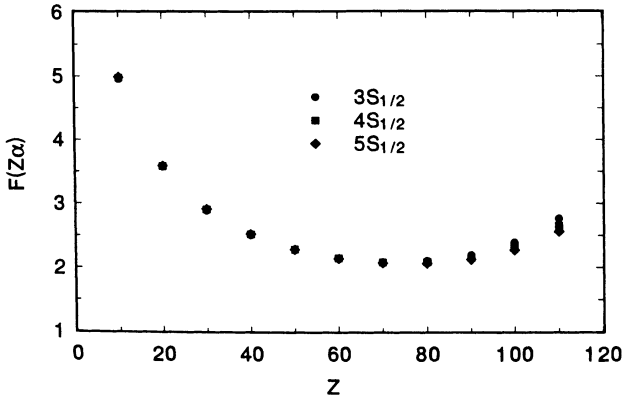

FIG. 1. The function $F(Z\alpha)$ for $S_{1/2}$ states with $n = 3, 4, 5$.

$$f_1(x) = N^{1/2}(1 + E)^{1/2} \times \sum_{m=0}^{n_r} \left(C_1^{(m)} + C_2^{(m)}\right)(2ax)^{m+\lambda-1} e^{-ax} \tag{A7}$$

and

$$f_2(x) = N^{1/2}(1 - E)^{1/2} \times \sum_{m=0}^{n_r} \left(C_1^{(m)} - C_2^{(m)}\right)(2ax)^{m+\lambda-1} e^{-ax}. \tag{A8}$$

The momentum-space radial wave functions $g_1(p)$ and $g_2(p)$ defined by

$$\varphi(\mathbf{p}) = \frac{1}{(2\pi)^{3/2}} \int d\mathbf{x}\, e^{-i\mathbf{p}\cdot\mathbf{x}} \phi(\mathbf{x}) = \begin{pmatrix} g_1(p)\chi_\kappa^\mu(\hat{\mathbf{p}}) \\ g_2(p)\chi_{-\kappa}^\mu(\hat{\mathbf{p}}) \end{pmatrix} \tag{A9}$$

are given by

$$g_1(p) = e^{i\theta_\kappa} \left(\frac{2}{\pi}\right)^{1/2} \int_0^\infty dx\, x^2 j_{l(\kappa)}(px) f_1(x) \tag{A10}$$

and

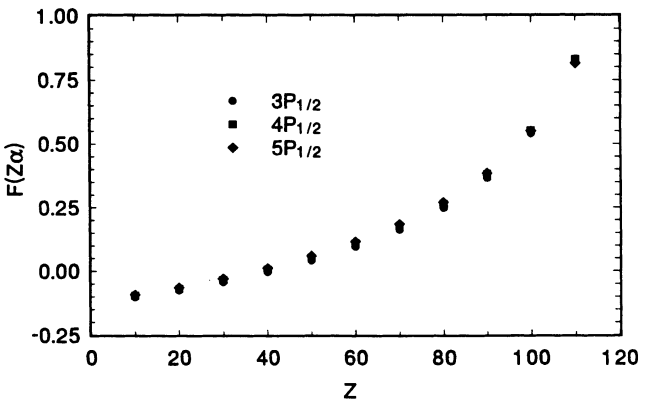

FIG. 2. The function $F(Z\alpha)$ for $P_{1/2}$ states with $n = 3, 4, 5$.

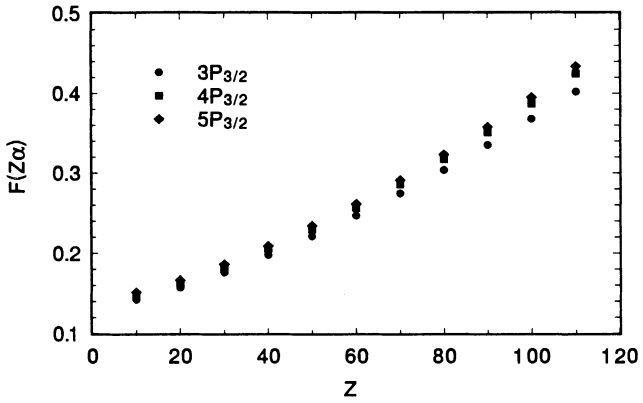

FIG. 3. The function $F(Z\alpha)$ for $P_{3/2}$ states with $n = 3, 4, 5$.

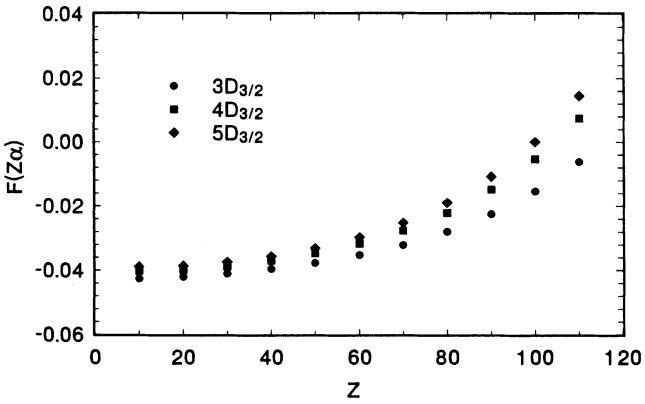

FIG. 4. The function $F(Z\alpha)$ for $D_{3/2}$ states with $n = 3, 4, 5$.

$$g_2(p) = -e^{i\theta_\kappa}\frac{\kappa}{|\kappa|}\left(\frac{2}{\pi}\right)^{1/2}\int_0^\infty dx\; x^2 j_{l(-\kappa)}(px) f_2(x), \tag{A11}$$

where $j_{l(\kappa)}$ is the spherical Bessel function with subscript $l(\kappa) = |\kappa + \frac{1}{2}| - \frac{1}{2}$, and θ_κ is a phase that is replaced by zero in the calculation. A recursion relation in l for the integrals that appear in (A10) and (A11),

$$D_l^{(m)} = \left(\frac{2}{\pi}\right)^{1/2}\int_0^\infty dx\; x^2 j_l(px)(2ax)^{m+\lambda-1}e^{-ax}, \tag{A12}$$

is readily obtained by substituting the right-hand side of

$$j_{l+1}(x) = \frac{l}{x}\, j_l(x) - \frac{d}{dx}\, j_l(x) \tag{A13}$$

into the expression for $D_{l+1}^{(m)}$ and integrating by parts to eliminate the derivative in the second term. The resulting relation is

$$pD_{l+1}^{(m)} = (l + m + \lambda + 1)2aD_l^{(m-1)} - aD_l^{(m)} \tag{A14}$$

with the initial value

$$D_0^{(m)} = \frac{(2a)^{m+\lambda}\Gamma(m+\lambda+1)}{(2\pi)^{1/2}} \times \frac{\sin\left[(m+\lambda+1)\tan^{-1}\left(\frac{p}{a}\right)\right]}{ap(a^2+p^2)^{(m+\lambda+1)/2}}. \tag{A15}$$

In terms of this expression, the wave functions are

$$g_1(p) = e^{i\theta_\kappa}N^{1/2}(1+E)^{1/2} \times \sum_{m=0}^{n_r}\left(C_1^{(m)} + C_2^{(m)}\right) D_{l(\kappa)}^{(m)} \tag{A16}$$

and

$$g_2(p) = -\, e^{i\theta_\kappa}\frac{\kappa}{|\kappa|}N^{1/2}(1-E)^{1/2} \times \sum_{m=0}^{n_r}\left(C_1^{(m)} - C_2^{(m)}\right) D_{l(-\kappa)}^{(m)}. \tag{A17}$$

Similarly, the functions $(Vg)_1(p)$ and $(Vg)_2(p)$, defined by

$$(V\varphi)(\mathbf{p}) = \frac{1}{(2\pi)^{3/2}}\int d\mathbf{x}\; e^{-i\mathbf{p}\cdot\mathbf{x}}V(\mathbf{x})\phi(\mathbf{x}) = \begin{pmatrix}(Vg)_1(p)\;\chi_\kappa^\mu(\hat{\mathbf{p}})\\ (Vg)_2(p)\;\chi_{-\kappa}^\mu(\hat{\mathbf{p}})\end{pmatrix}, \tag{A18}$$

where $V(\mathbf{x}) = -\gamma/x$, are given by

$$(Vg)_1(p) = -\, e^{i\theta_\kappa}N^{1/2}(1+E)^{1/2} \times \sum_{m=0}^{n_r}\left(C_1^{(m)} + C_2^{(m)}\right) 2a\gamma D_{l(\kappa)}^{(m-1)} \tag{A19}$$

and

$$(Vg)_2(p) = e^{i\theta_\kappa}\frac{\kappa}{|\kappa|}N^{1/2}(1-E)^{1/2} \times \sum_{m=0}^{n_r}\left(C_1^{(m)} - C_2^{(m)}\right) 2a\gamma D_{l(-\kappa)}^{(m-1)}. \tag{A20}$$

APPENDIX B

The functions A_κ^{ij} that appear in (3.2) are given here for $D_{3/2}$ states ($\kappa_n = 2$). They are readily obtained from the expressions for $P_{3/2}$ states ($\kappa_n = -2$) with the aid of the symmetry expressed in Eq. (3.16) of Ref. [4] with the result

TABLE XIV. Comparison to Blundell and Snyderman [8] for the function $F(Z\alpha)$ at $Z = 80$.

State	Ref. [8]	This work
$3S_{1/2}$	2.102(5)	2.1018(1)
$3P_{1/2}$	0.248(5)	0.2483(1)
$3P_{3/2}$	0.304(5)	0.3038(1)
$3D_{3/2}$	−0.032(5)	−0.0279(1)
$4S_{1/2}$	2.08(1)	2.0840(1)
$4P_{1/2}$	0.27(1)	0.2649(1)
$4P_{3/2}$	0.32(1)	0.3170(1)

$$A_\kappa^{11}(x_2,x_1) = (E_n - z)|\kappa| \left(2\frac{d}{dy_2}\frac{d}{dy_1} + \frac{(2\kappa+1)(\kappa+1)}{y_2 y_1}\right) j_{l(\kappa)}(y_2) j_{l(\kappa)}(y_1), \tag{B1}$$

$$A_\kappa^{12}(x_2,x_1) = (E_n - z)|\kappa| \left[\frac{\kappa+1}{y_2}\left(-2\frac{d}{dy_1} + \frac{\kappa+1}{y_1}\right) j_{l(\kappa)}(y_2) j_{l(\kappa)}(y_1) + \left(2 + \frac{6}{y_1}\frac{d}{dy_1} - 3\frac{\kappa(\kappa-1)}{y_1^2}\right) j_{l(-\kappa)}(y_2) j_{l(-\kappa)}(y_1)\right], \tag{B2}$$

$$A_\kappa^{21}(x_2,x_1) = (E_n - z)|\kappa| \left[\left(-2\frac{d}{dy_2} + \frac{\kappa+1}{y_2}\right)\frac{\kappa+1}{y_1} j_{l(\kappa)}(y_2) j_{l(\kappa)}(y_1) + \left(2 + \frac{6}{y_2}\frac{d}{dy_2} - 3\frac{\kappa(\kappa-1)}{y_2^2}\right) j_{l(-\kappa)}(y_2) j_{l(-\kappa)}(y_1)\right], \tag{B3}$$

$$A_\kappa^{22}(x_2,x_1) = 3(E_n - z)|\kappa| \left[[(2\kappa+1)(\kappa-1)+6]\frac{1}{y_2 y_1}\frac{d}{dy_2}\frac{d}{dy_1} - \left(\frac{(5\kappa+1)(\kappa-1)}{y_2^2} - 2\right)\frac{1}{y_1}\frac{d}{dy_1} - \left(\frac{(5\kappa+1)(\kappa-1)}{y_1^2} - 2\right)\frac{1}{y_2}\frac{d}{dy_2} + \frac{(\kappa-1)^2(2\kappa^2+\kappa+1)}{y_2^2 y_1^2} - \kappa(\kappa-1)\left(\frac{1}{y_2^2} + \frac{1}{y_1^2}\right) + \frac{2}{3}\right] j_{l(-\kappa)}(y_2) j_{l(-\kappa)}(y_1), \tag{B4}$$

where $y_i = (E_n - z)x_i$, $i = 1, 2$.

[1] P. J. Mohr, At. Data Nucl. Data Tables **29**, 453 (1983).
[2] W. R. Johnson and G. Soff, At. Data Nucl. Data Tables **33**, 405 (1985).
[3] P. Indelicato and P. J. Mohr, in *Atomic Physics 12*, edited by J. C. Zorn and R. R. Lewis (AIP, New York, 1991), p. 501.
[4] P. J. Mohr, Ann. Phys. (N.Y.) **88**, 26 (1974).
[5] P. J. Mohr, Ann. Phys. (N.Y.) **88**, 52 (1974).
[6] P. J. Mohr, Phys. Rev. A **26**, 2338 (1982).
[7] Y.-K. Kim, D. H. Baik, P. Indelicato, and J. P. Desclaux, Phys. Rev. A **44**, 148 (1991).
[8] S. A. Blundell and N. J. Snyderman, Phys. Rev. A **44**, 1427 (1991).
[9] K. T. Cheng, W. R. Johnson, and J. Sapirstein, Phys. Rev. Lett. **66**, 2960 (1991).
[10] G. E. Brown, J. S. Langer, and G. W. Schaefer, Proc. R. Soc. London Ser. A **251**, 92 (1959).
[11] M. E. Rose, *Relativistic Electron Theory* (Wiley, New York, 1961).